Available online at www.sciencedirect.com
ScienceDirect
Journal of the European Ceramic Society 31 (2011) 1325–1332
www.elsevier.com/locate/jeurceramsoc

Microstructural and mechanical evaluation of porous biomorphic silicon carbide for high temperature filtering applications

M.A. Bautista [a], J. Quispe Cancapa [b], J. Martinez Fernandez [a,*], M.A. Rodríguez [c], M. Singh [d]

[a] *Dpto. de Física de la Materia Condensada-Instituto de Ciencia de Materiales, Universidad de Sevilla-CSIC, Sevilla 41080, Spain*
[b] *Biomorphic-EBT S.L., Sevilla, Spain*
[c] *I. de Ceramica y Vidrio, CSIC, 28049 Cantoblanco, Madrid, Spain*
[d] *Ohio Aerospace Institute, 22800 Cedar Point Road, Cleveland, OH 44142, USA*

Available online 3 August 2010

Abstract

Biomorphic SiC (bioSiC) is a low cost SiC/Si composite obtained by melt infiltration of carbon preforms obtained from the pyrolysis of cellulose precursors. The porosity and pore size distribution of bioSiC can be tailored for specific applications by adequate selection of the wood precursor. Natural and artificial industrial woods were explored as possible bioSiC precursors. Silicon was removed by chemical etching. Relevant microstructural parameters such as pore size distribution, total porosity, and permeability were characterized. Since the filtration process involves large pressure gradients along the material at high temperatures, mechanical properties of porous bioSiC from the different precursors were evaluated at room temperature and 800 °C. The feasibility of porous bioSiC as a filtration material for high temperature gasification processes is discussed in terms of these properties. MDF-bioSiC is shown to be a promising material for such applications because of its good mechanical properties, interconnected porosity, pore sizes, and permeability.

Keywords: Biomorphic SiC; Porosity; Permeability; Bending strength; Filtering

1. Introduction

Hot gas clean-up technology is a crucial element of advanced clean coal and fuel cell technologies, which are prime candidates for the electrical-power generation because of their high efficiency and low emission characteristics.[1–5] An essential process of these technologies is the expansion of hot pressurized gas through a gas turbine. Although these technologies are the cleanest and most efficient options for generating electricity from coal and carbonaceous waste materials, they require varying degrees of development and validation before being connected to power distribution grids. One of the main problems is cleaning the product gas to prevent excessive emission and/or damage to the power conversion equipment.

High process temperatures, while beneficial for cycle efficiency, impose severe limitations on the mechanical durability and corrosion resistance of component on the gas cleaning unit. This leads to the requirement of new filtration materials, which are radically different from those that are currently available for use at low temperature and/or ambient pressures. The most efficient way of separating particles at high temperature is to use ceramic filters. High temperature filtration systems which show promising properties include silicon carbide, silicon nitride, ceramic composites, and ceramic fabrics.[4–18]

Biomorphic silicon carbide (bioSiC) is a SiC-based advanced ceramic material, fabricated through a cost effective and environment friendly process, which uses cellulose as starting precursor. BioSiC shows excellent thermo-mechanical performance, chemical and structural stability, in a wide range of temperatures.[19–25] By careful selection of starting precursors, it is also possible to tailor the total porosity, pore size, interconnectivity, thermal and electrical properties to a wide range of values to satisfy device requirements. The aim of this study is to explore the feasibility of porous bioSiC as a filtration material in high temperature gasification processes.

2. Experimental procedures

2.1. Fabrication

BioSiC samples were fabricated using Sipo wood (Entandrophragma Utile) and medium density fiberboard as a starting

* Corresponding author. Tel.: +34 954552894.
E-mail address: martinez@us.es (J.M. Fernandez).

0955-2219/$ – see front matter © 2010 Elsevier Ltd. All rights reserved.
doi:10.1016/j.jeurceramsoc.2010.06.014

precursor (sipo-bioSiC, and MDF-bioSiC, respectively), by utilizing a process previously described elsewhere.[19–25] In brief, samples of wood were pyrolyzed in a flowing Ar atmosphere at 1000 °C (0.5 °C/min heating rate). Afterward, porous carbon samples of different dimensions were cut to prepare samples for mechanical testing and microstructural characterization. Carbon samples were also machined using a computer controlled machining equipment to obtain disks for the permeability tests. In the case of sipo-bioSiC, the disks were machined with the former axial wood direction perpendicular to the disk plane.

Carbon samples were infiltrated with liquid Si (Silgrain HQ-99.7% purity; Elkem Silicon, Oslo, Norway) at 1550 °C in vacuum. Samples were made in batches, each carbon precursor was covered with Si and a Si/C weight ratio of 3.2 was used. This ratio is higher than stoichiometrically needed for conversion. However, it was chosen to ensure the complete conversion of C into SiC since there is silicon loss at high temperatures due to high vapor pressure of silicon. The solid silicon, present on the sample surfaces after the infiltration step, was removed by mechanical grinding. No bulk volume increase was observed during the infiltration process.

The final product was a Si/SiC composite in which the SiC retain the microstructure of the cellulose based precursor. In order to eliminate silicon, wet chemical etching was performed on bioSiC using a HF/HNO_3 mixture at a molar ratio of 1.66 in water.[24] The chemical reactions during the etching process are as follows:

$$3Si + 4HNO_3 \rightarrow 3SiO_2 + 4NO + 2H_2O$$

$$SiO_2 + 4HF \rightarrow SiF_4 + 2H_2O$$

A porous silicon carbide scaffold was obtained after chemical etching. Etching times up to 72 h were used in order to study the rate of silicon removal, as well as the evolution of porosity and permeability.

2.2. Microstructural characterization

Microstructure observations were carried out using a Philips XL30 scanning electron microscope with secondary and back scattering electron detectors (CITIUS, University of Seville, Spain). Samples were prepared using conventional metallographic techniques.

Ashes obtained from a conventional ceramic filter of a biomass gasification process were also analyzed in order to evaluate the particle size to be filtered. This date will be helpful in designing the high temperature filters fabricated from bioSiC. The particle size was studied by image analysis of scanning electron microscopy micrographs and using a particle size analyzer (Mastersizer S, Malvern, UK).

2.3. Porosity and permeability measurements

Mercury porosimetry (PORO SIZER 9300, Micromeritics, USA) was used for the determination of the pore size and total porosity of the silicon carbide scaffolds obtained after chemical etching.

The cross flow experiments were performed using a homemade apparatus described elsewhere.[26] The permeability was measured on disks of 25 mm in diameter and 2 mm thickness made from sipo-bioSiC and MDF-bioSiC, etched up to 72 h.

The structural study of the filter was performed using the permeability method developed by Uhlhorn et al.[27] and later by Conesa et al.,[26] which can be summarized as follow.

The gas flow equation through a porous material is given by

$$\frac{NRT}{\nu \Delta P} = \frac{ko}{L} + \frac{Bo P_m}{L \eta \nu} \quad (1)$$

where N is the gas flow per unit area; R, gas constant; T, temperature; ΔP, pressure difference; $\nu = \sqrt{8RT/\pi M}$ the mean molecular velocity; M, the gas molecular weight; $ko = (2\varepsilon/3\tau)r_p$, the term corresponding to Knudsen diffusion; ε, the porosity; τ, tortuosity; r_p, pore radius; L, sample thickness; $Bo = (\varepsilon/8\tau)r_p^2$, the term corresponding to viscous flow; P_m is the mean pressure and η, gas viscosity.

The permeability (F) of a gas through a membrane is defined as the gas flow per unit area and per unit of the pressure difference

$$F = \frac{N}{\Delta P} \quad (2)$$

Substituting Eq. (2) in Eq. (1) is obtained a first degree equation$F = a + bP_m$where a is a constant corresponding to Knudsen diffusion; b, constant representing viscous flow and P_m, mean pressure. Knudsen diffusion is the transport mechanism when the pore diameters are smaller than the mean free paths of the molecules and it becomes important in membranes with small pore diameters.[28,29] In this case the permeability will not be function of the mean pressure. The transport by viscous flow (Poiseuille flow) arises when the pore diameter is bigger than the mean free paths of the molecules[30] yielding a pressure dependence on the permeability.

In order to study the permeability and mechanical robustness of larger samples, to be further used in a prototype device inserted in a biomass gasification plant, a homemade device was designed and fabricated. In this device, disks of 78 mm in diameter and 2.5 mm thickness made from the selected precursors and etched for optimum times, were inserted in sealed steel clamps in which gas pressure and gas flow input are controlled, and gas pressure and gas flow output are also measured. Gas flow versus pressure difference was measured and permeability was determined.

2.4. Mechanical characterization

Bending tests were carried out at room temperature and 800 °C, at a constant strain rate of 0.5 mm/min using a screw-driven universal testing machine (Microtest EM1/50/FR, Madrid, Spain). The load was applied using alumina rods, which were protected from direct contact with the bending fixture by sintered SiC pads. The sections in contact with the SiC pads were ground flat parallel. 5 mm × 6 mm × 60 mm bioSiC samples were fabricated, etched at different times and tested up to failure.

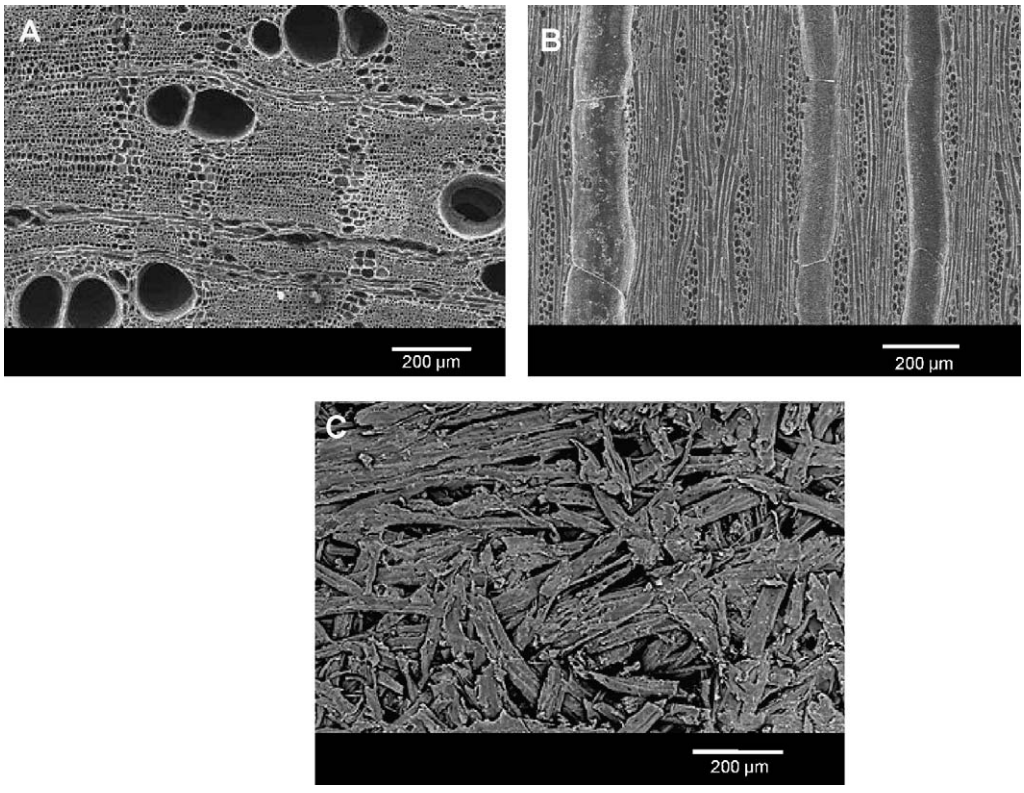

Fig. 1. Back scattering SEM micrographs of: (A) pyrolized sipo wood in the axial plane, (B) pyrolized sipo wood in the longitudinal plane, and (C) pyrolized MDF.

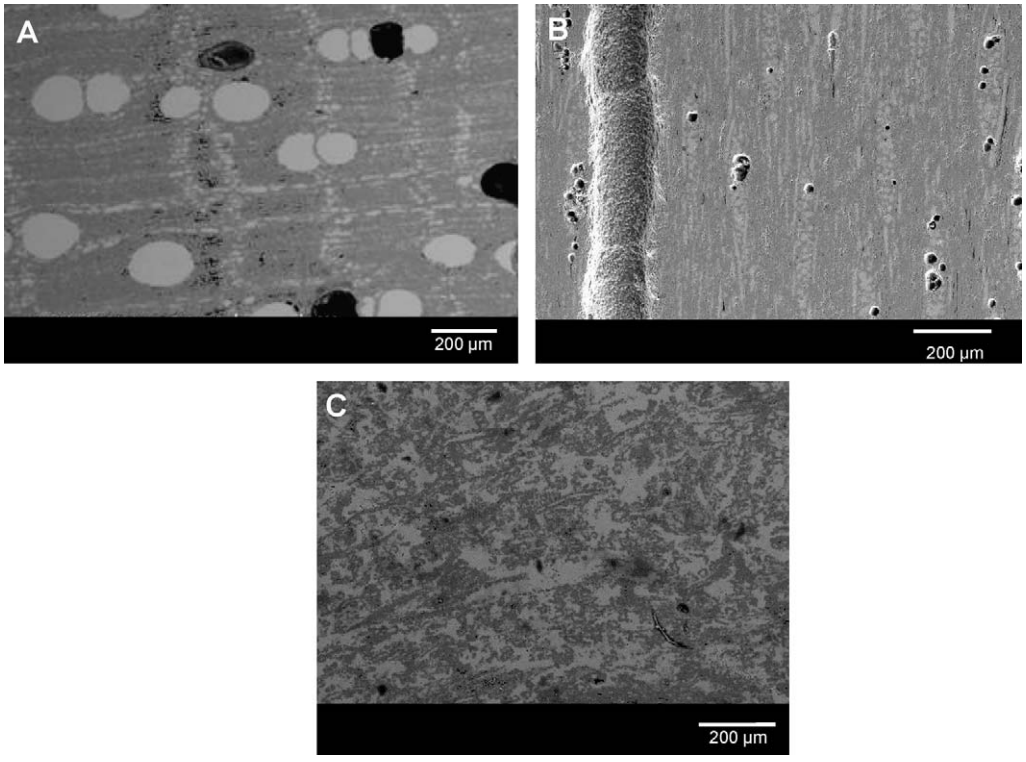

Fig. 2. Back scattering SEM micrographs of: (A) sipo-bioSiC in the axial plane, (B) sipo-bioSiC in the longitudinal plane, and (C) MDF-bioSiC.

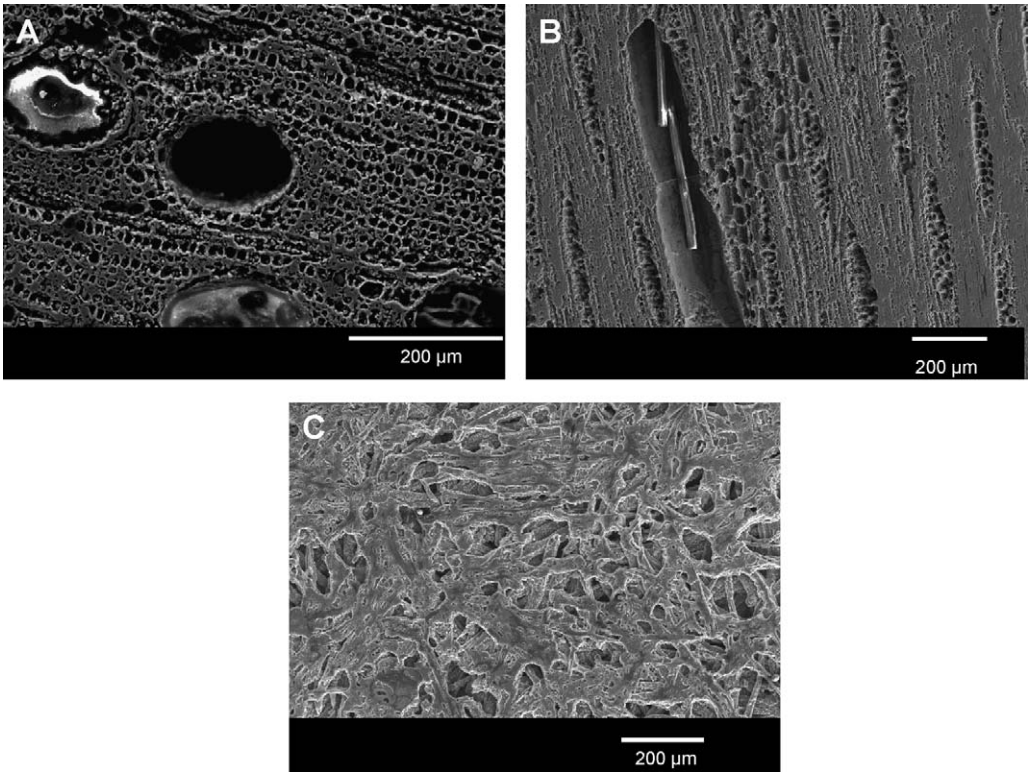

Fig. 3. Back scattering SEM micrographs of: (A) porous sipo-bioSiC in the axial plane, (B) porous sipo-bioSiC in the longitudinal plane, and (C) porous MDF-bioSiC. All materials have been etched for 1 h.

3. Results and discussion

The microstructure of the carbon performs obtained by the pyrolysis of the wood based precursors is shown in Fig. 1. The channel structure typical of hard woods is clearly identified on the carbon obtained from sipo wood (Fig. 1A and B). The carbon obtained from MDF also maintains the fiberboard microstructure consisting in a compact of cellulose fibers.

The microstructure of the Si/SiC composites is shown in the back scattering SEM micrographs of Fig. 2. It is also evident how the SiC phase (darker) mimics the precursor microstructure. The lighter phase is silicon and fills up the pores of the SiC structure. The microstructure also shows very little presence of unreacted carbon, that has high contrast (dark).

The chemical etching described above progressively eliminates silicon. In the micrographs of Fig. 3, details of the SiC porous scaffolds obtained after 1 h etching are shown. The anisotropic advance of etching front, and weight loss as a function of the chemical etching on bioSiC, has been characterized in detail in a previous publication.[31] In the case of porous sipo-bioSiC, the microstructure resembles that of the sipo wood, a combination of large channels optimized for fluids transport and small channels that give structural strength at low density. Porous MDF-bioSiC microstructure is more uniform and isotropic, corresponding with the microstructure of the wood fibers that compose the MDF precursor.

In Fig. 4 the pore size distributions for sipo-bioSiC etched 1, 24, and 48 h are presented. The pore size distribution is bimodal, with small pores with sizes ranging roughly from 0.2 to 10 with µm, and very large pores/channels with sizes ranging between 50 and 250 µm. Table 1 presents the porosity, peak pore size and pore size range for each material studied. For etching times up to 7 h, the large channels of the SiC network are still filled up with silicon and the largest pores have sizes of approximately 100 µm. For longer etching times the volume of large pores increases dramatically, with sizes up to 250 µm. Despite the scatter on the data, due to the non-uniformity of the microstructure, it can be concluded that the large pores will be controlling the gas flow and filtering capabilities of this material.

Fig. 5 shows the pore size distributions for MDF-bioSiC etched 3, 24, and 72 h. Table 2 presents the porosity, peak pore

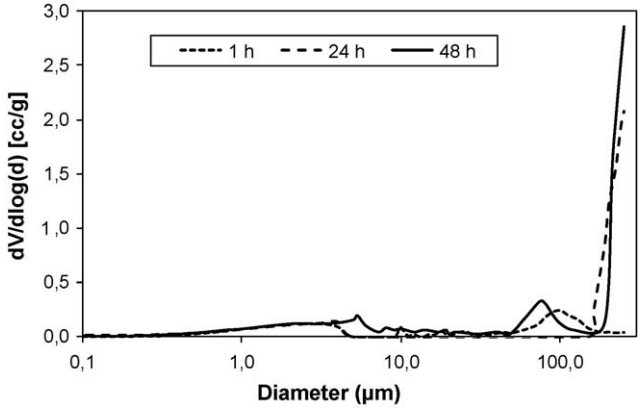

Fig. 4. Pore size distribution of sipo-bioSiC after 1, 24, and 48 h of etching.

Table 1
Microstructural parameters and permeability range of sipo-bioSiC for different etching times.

Etching time (h)	Porosity (%)	Pore size range (μm)	Main peak pore (μm)	Permeability range (pressure range 1.7–4.0 × 10^6 dina/cm^2)
1	32	0.2–5, 10–200	~3, 100	1.0–3.5 × 10^{-4} cm^3/s dina
4	37	0.2–10, 10–200	~4, 100	0.9–1.7 × 10^{-4} cm^3/s dina
7	30	0.2–10, 20–200	~4, 110	1.0–1.6 × 10^{-4} cm^3/s dina
24	50	0.2–10, 50–250	~4, 250	3.8–6.0 × 10^{-4} cm^3/s dina
48	75	0.2–20, 50–250	~5, 250	3.8–5.4 × 10^{-4} cm^3/s dina

Table 2
Microstructural parameters and permeability range of MDF-SiC for different etching times.

Etching time (h)	Porosity (%)	Pore size range (μm)	Peak pore size (μm)	Permeability range (pressure range 1.8–4.0 × 10^6 dina/cm^2)
3	43	0.2–30	~20	2.7–3.9 × 10^{-5} cm^3/s dina
9	48	0.2–30	~20	2.0–3.5 × 10^{-5} cm^3/s dina
24	48	0.2–30	~20	2.7–3.6 × 10^{-5} cm^3/s dina
48	49	0.2–30	~20	3.0–5.0 × 10^{-5} cm^3/s dina
72	57	0.2–5, 5–18, 110–250	~3, 15, 250	1.5–2.5 × 10^{-5} cm^3/s dina

size, and pore size range for each material studied. The pore size distribution on the range of 0.2–30 μm for etching times up to 48 h, is considerable smaller that the pores of sipo-bioSiC. Only after 72 h of etching, large pores with sizes up to 250 μm are created. MDF-bioSiC presents a finer and uniform microstructure than sipo-bioSiC, up to very large etching times, which indicates that is a more feasible material for high temperature filtering applications.

The N_2 permeability as a function of mean pressure measured in sipo-bioSiC 25 mm × 2 mm disks is plotted in Fig. 6. The permeability ranges roughly between 1 and 6 × 10^{-4} cm^3/s dina, values that are higher than those of typical filtering membranes (approximately 0.2–2 × 10^{-5} cm^3/s dina),[16] being the pressures used in this work (1.7–4.0 × 10^6 dina/cm^2) lower than the ones used in Ref. 16 (4–20 × 10^7 dina/cm^2). The permeability ranges are presented in Table 1 for each etching time. For 1 h etched samples the increase of mean pressure results on an increase on permeability, and the pressure drop on the disk ranges from 1 to 5 × 10^4 dina/cm^2 for gas pressures ranging from 1.7 to 3.8 × 10^6 dina/cm^2. For this etching time the large channels are not fully open (silicon is not completely removed), but transport may be occurring by viscous flow (Knudsen diffusion is out of the question because the pore size is larger than the mean free paths of the molecules for all the materials studied in this work), what would explains the dependence of permeability with mean pressure. For 24 and 48 h of etching, the pressure drop is very small for the range of pressures used, and the permeability larger than for samples etched for 1 h, what is probably associated to the large pores and their alignment. The permeability for these two etching times has an anomalous decrease with mean pressure that is under study.

The N_2 permeability as a function of mean pressure in MDF-bioSiC 25 mm × 2 mm disks is plotted in Fig. 7. The permeability ranges roughly between 1 and 5 × 10^{-5} cm^3/s dina, values that are in the range of those of typical filtering membranes.[16] The permeability ranges are also presented in Table 2 for each etching time. The permeability increases with mean pressure, probably because the effect of viscous flow is important. The smaller pore size and the tortuosity of the flow path in MDF-bioSiC results in a larger pressure drop that ranges from 1 to 4 × 10^5 dina/cm^2 for mean pressures ranging from 1.8

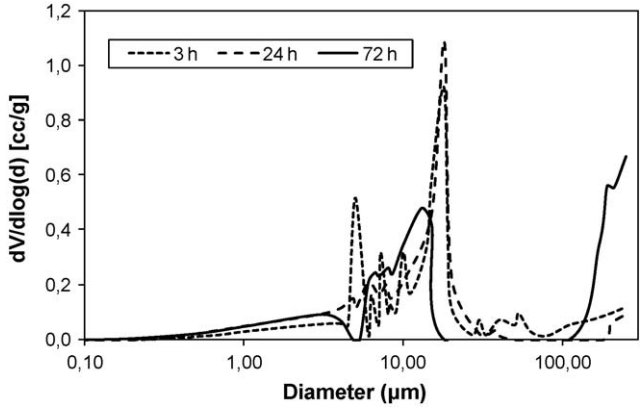

Fig. 5. Pore size distribution of MDF-bioSiC after 3, 24, and 72 h of etching.

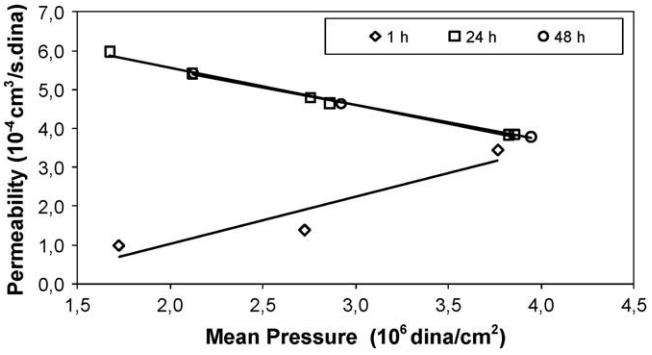

Fig. 6. Permeability as a function of mean pressure of sipo-bioSiC with different etching times.

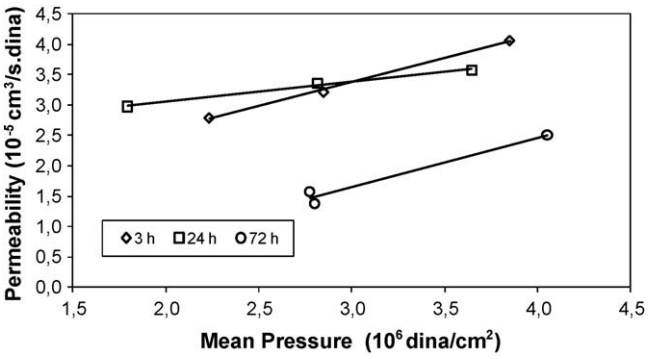

Fig. 7. Permeability as a function of mean pressure of MDF-bioSiC with different etching times.

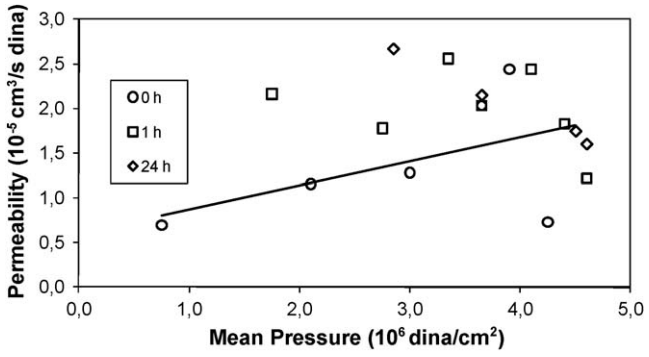

Fig. 8. Permeability versus mean pressure of MDF-bioSiC large disks with different etching times. The linear fit for the data of the unetched samples is inserted.

to 4.0×10^6 dina/cm^2. Due to this microstructure, the permeability in MDF-bioSiC is one order of magnitude smaller that in sipo-bioSiC, despite the fact that the total porosity is very similar.

Larger samples (78 mm × 2.5 mm disks) of MDF-bioSiC were studied. Fig. 8 shows the plot of the permeability versus mean pressure for a range of etching times. The range of permeability ($0.7–2.6 \times 10^{-5}$ cm^3/s dina) corroborate the values obtained in the study of smaller disks. The pressure drop is higher (ranges from 2 to 8×10^5 dina/cm^2 for mean pressures ranging from 0.8 to 4.6×10^6 dina/cm^2) due to the larger thickness. It is interesting also to note that samples that have not been etched have a significant permeability. A slight increase

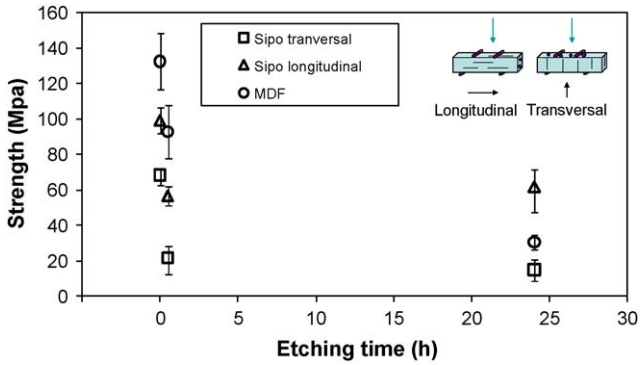

Fig. 10. Bending strength at room temperature versus etching time (0, 0.5 and 25 h) of sipo and MDF-bioSiC. Test configuration is inserted.

of permeability with mean pressure can be detected in some cases, like in the unetched MDF-bioSiC (fit line inserted on plot), but for longer etching times (larger pores) there was not clear dependence. All disks were robust and did not undergo mechanical failure during the permeability measurements. In summary, these measurements give us the range of permeability and pressure drops expected from these materials and some insights on their dependence with mean pressure.

Ashes obtained from gasification process filters were studied to determine their particle size distribution, and to evaluate the feasibility of building bioSiC filters that can retain these particles. It is especially important to determine the size of the smallest particles, which will determine the critical pore size on the filters. The SEM micrograph of Fig. 9A shows the morphology of the smallest particles. Their average diameter is on the range of 1 μm (1.3 ± 0.7 μm). The results obtained with a particle size analyzer give the grain size distribution of Fig. 9B. The smallest particle sizes are approximately one micron, in good agreement with the SEM observations.

The mechanical strength of sipo-bioSiC and MDF-bioSiC as a function of etching time (0, 0.5, and 24 h) was determined by bending tests at room temperature and 800 °C (Figs. 10 and 11, respectively). There are previous studies of the compressive strength of these materials for a wide range of etching time and temperatures.[31] In this work, we complete these previous results with data obtained in the most unfavorable conditions: high temperature, silicon etched away, and load application by bending.

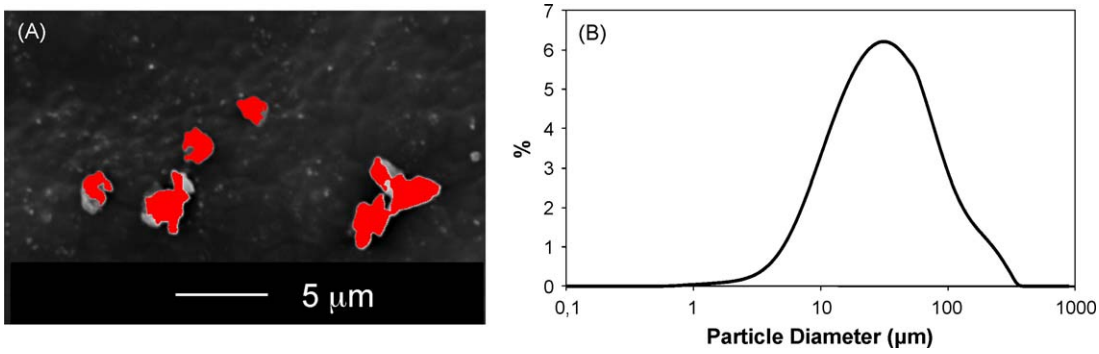

Fig. 9. (A) Scanning electron microscopy micrograph, and (B) particle size distribution of ashes generated during gasification process.

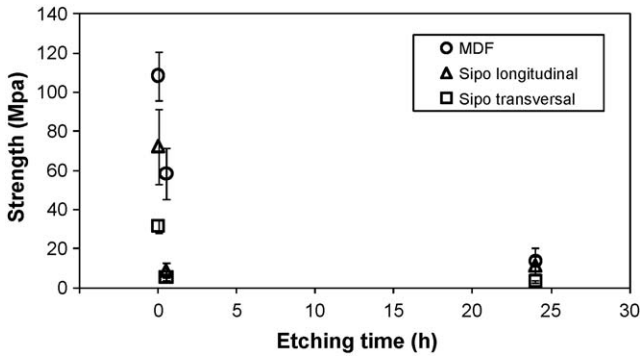

Fig. 11. Bending strength at 800 °C versus etching time (0, 0.5 and 25 h) of sipo and MDF-bioSiC. Test configuration is inserted in Fig. 10.

MDF-bioSiC is stronger than sipo-bioSiC at room temperature (133 ± 16 MPa and 99 ± 5 MPa, respectively) and 800 °C (109 ± 12 MPa and 72 ± 19 MPa, respectively), and undergoes smaller strength degradation after 0.5 h of etching. In addition sipo-bioSiC presents an important anisotropy that is detrimental for the mechanical properties and filter design. After 24 h of etching, the strength of both materials degraded to approximately the same value. Porous MDF-bioSiC obtained with 0.5 h of etching could have a microstructure suitable for filtering applications and be robust enough, with a bending strength of 93 ± 15 MPa at room temperature and 59 ± 13 MPa at 800 °C.

4. Conclusions

The feasibility of porous bioSiC for application as high temperature filters was evaluated. Porous silicon carbide based materials were successfully fabricated from medium density fiberboard (MDF) and natural sipo wood. The porosity of sipo-bioSiC materials ranged from 32% to 75% with characteristic bimodal distribution of pore sizes, and a large volume fraction of pores with sizes over 100 μm. The porosity MDF-bioSiC materials ranged from 43% to 57% with characteristic pore size around 10–20 μm.

The permeability of porous MDF-bioSiC was in the range of $1–5 \times 10^{-5}$ cm^3/s dina for a pressure range of $2–4 \times 10^6$ dina/cm^2. For a similar pressure range the permeability of sipo-bioSiC was in the range of $1–6 \times 10^{-4}$ cm^3/s dina. The considerably larger permeability of porous SiC fabricated from sipo wood is related with the existence of interconnected larger size channels/pores with preferred orientation, more than with the total porosity value. Permeability increases with mean pressure for the MDF-bioSiC materials and for the smaller pore size sipo-bioSiC, probably because the transport is occurring by viscous flow. The smaller pore size and the tortuosity of the flow path in MDF-bioSiC results in a larger pressure drops. Tests on larger samples demonstrate the structural stability of MDF-bioSiC to be used on filtering applications and corroborate the range of permeability and pressure drops. Bending tests show that MDF-bioSiC has a better mechanical behavior than sipo-bioSiC at room temperature and 800 °C.

The study of the microstructure, mechanical properties and permeability of MDF-bioSiC with short etching times indicates that this material is the best candidate for filtering applications, because it presents interconnected uniforms porosity, pores sizes and permeability in an adequate range, and structural strength.

Acknowledgements

The authors acknowledge the financial support of the Spanish Ministerio de Ciencia e Innovación (BIOFIL project, CIT-120000-2008-16).

References

1. Brown TD. Coal gasification-combined cyc1es for electricity production. *Prog Energy Combos Sci* 1982;**8**:277–301.
2. Schmoe LA, Lennox FH. Gasification combined cycle economics. In: Cooke DH, Borglin SH, Holland HW, Langston LS, editors. *1992 ASME COGEN-TURBO, 6th international conference in cogeneration and utility industrial and independent power generation*. New York: American Society of Mechanical Engineers; 1992. p. 179–85.
3. Vlaswinkel EE. Energetic analysis and optimization of an integrated coal gasification-combined cyc1e power plant. *Fuel Process Technol* 1992;**32**:47–67.
4. Newby RA, Bannister RL. Advanced hot gas cleaning system for coal gasification processes. *J Eng Gas Turbines Power* 1994;**116**:338–44.
5. Dahlin RS, Pontius DH, Haq ZU, Vimalchand P, Brown R, Wheeldon J. Plans for hot gas c1eanup testing at the power systems development facility. In: Heinschel KJ, editor. *Proceedings of the thirteenth international conference on fluidized bed combustion, vol. 1*. New York: American Society of Mechanical Engineers; 1995. p. 449–59.
6. Sellakumar KM, Isaksson JSJ, Provol SJ. High pressure high temperature gas cleaning using an advanced ceramic tube filter. In: Anthony EJ, editor. *Proceedings of the eleventh international conference on fluidized bed combustion, vol. 2*. New York: American Society of Mechanical Engineers; 1991. p. 1087–95.
7. Corbitt N. *Inorganic membranes: markets, technologies, players*. Business Communications Company, Inc.; 1997.
8. Burggraaf AJ, Keizer K. *Inorganic membranes: synthesis, characteristics and applications*. New York: Chapman & Hall; 1991. p. 11–63.
9. Vercauteren S, Keyzer K, Vansant EF, Luyten J, Leysen R. Porous ceramic membranes: preparation, transport properties and applications. *J Porous Mater* 1998;**5**:241–58.
10. Benito JM, Conesa A, Rodríguez MA. Membranas cerámicas. Tipos, métodos de obtención y caracterización. *Bol Soc Ceram V* 2004;**5**:821–34.
11. Tsuru T. Inorganic porous membranes for liquid phase separation. *Sep Purif Methods* 2001;**30**:191–220.
12. Cot L, Ayral A, Durand J, Guizard C, Hovnanian N, Julbe A. Inorganic membranes and solid state sciences. *Solid State Sci* 2000;**2**:313–34.
13. Guizard C. In: Burggraaf AJ, Cot L, editors. *Fundamentals of inorganic membrane science and technology*. The Netherlands: Elsevier B.V.; 1996. p. 227–58.
14. Gestel TV, Vandecasteele C, Buekenhoudt A, Dotremont C, Luyten J, Leysen R. Alumina and titania multilayer membranes for nanofiltration: preparation, characterization and chemical stability. *J Membr Sci* 2002;**207**:73–89.
15. Ariza MJ, Cañas A, Rodríguez-Castellón E, Cabeza A, Benavente J. Modificación de una membrana de alúmina (g-Al2O3): caracterización mediante parámetros electroquímicos y espectroscopía de fotoelectrones de rayos X. *Bol Soc Ceram V* 2002;**41**:122–5.
16. Benito JM, Conesa A, Rubio F, Rodríguez MA. Preparation and characterization of tubular ceramic membranes for treatment of oil emulsions. *J Eur Ceram Soc* 2005;**25**:1895–903.
17. Benito JM, Conesa A, Rodríguez MA. Preparation of multilayer ceramic systems for deposition of mesoporous membranes. *J Mater Sci* 2005;**40**:6105–12.
18. Adler J. Ceramic diesel particulate filters. *Int J Appl Ceram Technol* 2005;**2**(6):429–39.

19. Martinez-Fernandez J, Valera-Feria FM, Singh M. High temperature compressive mechanical behavior of biomorphic silicon carbide ceramics. *Scripta Mater* 2000;**43**:813–8.
20. Martínez-Fernández J, Valera-Feria FM, Domínguez Rodríguez A, Singh M. Microstructure and thermomechanical characterization of biomophic silicon carbide-based ceramics. In: *Environment conscious materials. Ecomaterials*. Canadian Institute of Mining, Metallurgy, and Petroleum; 2000, ISBN 1-894475-04-6. p. 733–740.
21. Singh M, Martínez-Fernández J, de Arellano-López AR. Environmentally conscious ceramics (ecoceramics) from natural wood precursors. *Curr Opin Solid State Mater Sci* 2003;**7**:247–54.
22. de Arellano-López AR, Martínez-Fernández J, González P, Domínguez C, Fernández-Quero V, Singh M. Biomorphic SiC: a new engineering ceramic material. *Int J Appl Ceram Technol* 2004;**1**(1):56–67.
23. Varela-Feria FM, Martinez-Fernandez J, de Arellano-Lopez AR, Singh M. Low density biomorphic silicon carbide: microstructure and mechanical properties. *J Eur Ceram Soc* 2002;**22**:2719–25.
24. Varela-Feria FM, Ramırez-Rico J, de Arellano-Lopez AR, Martınez-Fernandez J, Singh M. Reaction-formation mechanisms and microstructure evolution of biomorphic SiC. *J Mater Sci* 2008;**43**:933–41.
25. Bautista MA, de Arellano-Lopez AR, Martnez-Fernandez J, Bravo-Leon A, Lopez-Cepero JM. Optimization of the fabrication process for medium density fiberboard (MDF)-based biomimetic SiC. *Int J Refract Met Hard Mater* 2009;**27**:431–7.
26. Conesa A, Fernandez Roura A, Pitarch JA, Vicente-Mingarro I, Rodriguez MA. Separation of binary gas mixtures by means of sol–gel modified ceramic membranes. Prediction of membrane performance. *J Membr Sci* 1999;**155**:123–31.
27. Uhlhorn RJR, Huits In't Veld MHBJ, Keizer K, Burggraaf AJ.*First international conference on inorganic membranes*. 1989. p. 323–8.
28. Hwang S-T. Mechanisms of gas permeation through microporous membranes—a review. *Membr J* 1997;**7**:1–10.
29. Bitter JGA. *Transport mechanisms in membrane separation processes*. New York: Plenun Press; 1991. p. 2–9.
30. Ahmad AL, Othman MR, Mukhtar H. H_2 separation from binary gas mixture using coated alumina-titania membrane by sol–gel technique at high-temperature region. *Int J Hydrogen Energy* 2004;**29**:817–28.
31. Torres-Raya C, Hernandez-Maldonado D, Ramirez-Rico J, Garcia-Gañan C, de Arellano-Lopez AR, Martinez-Fernandez J. Fabrication, chemical etching and compressive strength of porous biomimetic SiC for medical implants. *J Mater Res* 2008;**23**:3247–54.